Moderated Poster Session I: Basic Science
Thursday, September 23: 4:00-5:00 p.m.

P1
Development of a Nanolantern™ Assay for Rapid Detection of *Enterobacter Cloacae*

Angelo J. Cambio,[1] *Jennifer G. Rothschild,*[1] *Hsin-P Peng,*[2] *Robert D. Mayer,*[1] *Benjamin L. Miller*[2]
[1]University of Rochester Medical Center, Rochester, NY, USA; [2]University of Rochester, Rochester, NY, USA

Background: Urinary tract infections (UTI) are among the most common bacterial infections in the United States. The gold standard for diagnosis is urine culture. This provides bacteria identification and sensitivity, but is labor intensive and time-consuming. As such, many UTIs are treated empirically contributing to resistance and cost. There is an urgent need for a diagnostic tool that can rapidly identify uropathogens and their sensitivities. We present the development of a PCR-based assay for *Enterobacter cloacae*, and evidence for its further use in the context of NanoLantern™ technology. The NanoLantern™ is a chip sensor that utilizes DNA hairpins immobilized onto a gold surface. In the presence of complementary (target) DNA, the hairpin stem is opened, exposing a quantifiable fluorophore.
Methods: A synthetic DNA hairpin, unique to *Enterobacter cloacae,* was immobilized onto 9 gold coated chips. Baseline fluorescence intensity was recorded. The chip was exposed to synthetic target and then imaged with a fluorescence microscope. Fluorescence intensity was recorded and compared to baseline. PCR, asymmetric PCR and linear after the exponential PCR were used to amplify the target DNA from the bacteria. The amplicon was exposed to the NanoLantern™ chip and fluorescence intensity was quantified.
Results: Pre-synthetic target fluorescence imaging of 9 chips exposed to synthetic DNA resulted in a mean raw count of 665 (SD ± 244). Post-synthetic target fluorescence imaging of 9 chips resulted in a mean raw count of 8197 (SD ± 648), a greater than 12-fold increase in intensity. See Fig. 1.
Conclusions: We have demonstrated the feasibility of a novel DNA hairpin probe. Work is ongoing to develop a PCR assay and to begin testing the NanoLantern™ chip with bacteria derived amplicon and urine samples. Ultimately, these integrated assays will provide rapid analysis, as part of an automated system, to be used in the clinical setting.

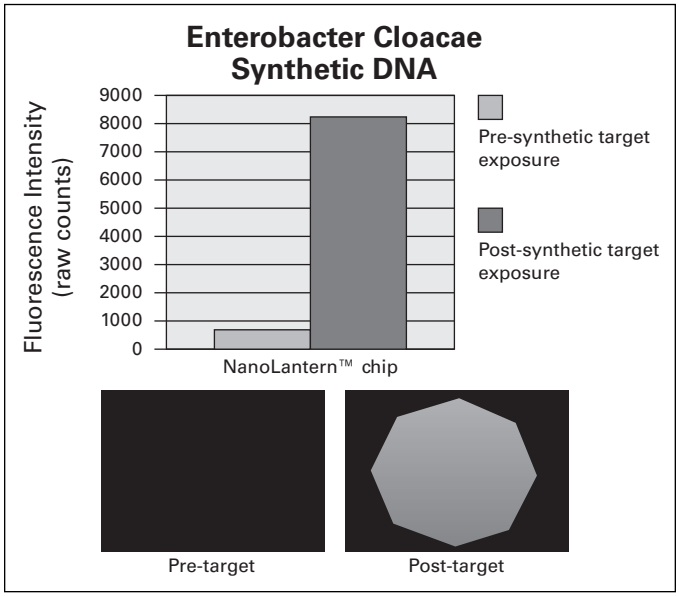

Fig. 1. P1. Fluorescence microscopy of chip pre- vs. post-target exposure.

P2
WITHDRAWN

P3
Nox4 Inhibitor as a Potential Therapeutic Agent for Renal Cell Carcinoma

Li Chen, *Guimin Chang, Jodi K. Maranchie*
University of Pittsburgh Medical Center, Pittsburgh, PA, USA

Background: Nox4 is a member of the NADP(H) oxidase enzyme family that transports electrons across biological membranes to produce reactive oxygen species (ROS). Loss of the von Hippel-Lindau tumor suppressor (VHL) leads to activation of hypoxia-inducible factor-2α (HIF-2α) with increased VEGF, Glut-1, TGF-α expression. We have shown that Nox4 is essential for HIF-2α transcriptional activity and that inhibition of Nox4 abrogates HIF transactivation in VHL-deficient renal cell cancer (RCC) cells. Therefore, Nox4 may serve as a therapeutic target to for RCC. To test this, we screened novel compounds with activity against Nox4 in a human VHL-deficiency renal cell carcinoma xenograft tumor model.
Methods: One million 786-O cells in 100 µl HBSS were injected subcutaneously in the left flank of 6-week-old female SCID Beige mice. Tumors were measured in two dimensions and estimated tumor weights were calculated using the formula: V (mm^3) = (length × $width^2$)/2. When tumors reached 100-150 mm^3, mice were stratified into 6 equal groups of 10 mice each. Compounds, GKT137892 (100 mg/kg), GKT137928 (100 mg/Kg), GKT136901 (100 mg/Kg) or sutent (40 mg/kg) were administrated by daily gavage for 34 days. Controls arms received no gavage or gavage with vehicle only. Mice were sacrificed at 24h after last gavage, and tumors were harvested and weighed. Significance was determined by ANOVA and Student T tests.
Results: Sutent inhibition of xenograft tumors was observed by day 1. GKT136901 treatment inhibited tumor growth by day 15. The average volume of the tumors in GKT136901-treated group was 208.36 mm^3 on day 22 of treatment vs 279.26 mm^3 and 275.24 mm^3 for the two control groups, respectively, representing a 26% growth inhibition ($p = 0.012$). For compounds, GKT137892 and GKT137928, no growth inhibition was seen. No toxicity was observed for any of the drugs.
Conclusions: GKT136901, an inhibitor of Nox4, inhibits 786-O cell xenograft tumor growth, providing proof of principle for Nox4 as a therapeutic target for RCC. Efficacy may be further enhanced by structural alterations that improve tumor penetration.

P4

A Dual Adenoviral Amplification System Based on PSA-promoter to Increase Sensitivity of Detection of Prostate Cancer Cells *In Vivo* By Non Invasive Imaging

Frederic Pouliot,[1] *Makoto Sato,*[2] *Lily Wu*[2]
[1]Université Laval, Québec, QC, Canada; [2]University of California, Los Angeles, Los Angeles, CA, USA

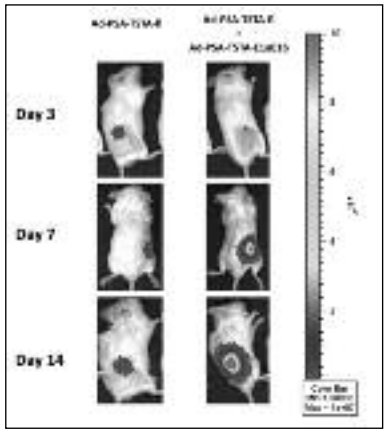

Fig. 1. P4.

Introduction and Objectives: When PSA recurs after prostatectomy, localization of prostate cancer cells by imaging is important to decide which patients should receive salvage radiation therapy (RT) as opposed to androgen deprivation therapies. However, the threshold at which prostate cancers cells must be detected for RT to be efficient is <1 ng/mL of serum PSA necessitating sensitive imaging tools. We have developed a dual transcriptional amplification system (DTSTA) that allows sensitive detection of prostate cells by non invasive imaging and tested it in a local recurrence prostate cancer model.

Methods: Adenovirus (Ad) expressing firefly luciferase (fl) under the control of a modified PSA promoter and the Two-Step-Amplification-Transcription system (Ad-PSATSTAfl) was constructed as previously described (Sato et al. 2008). We have also constructed an oncolytic adenovirus expressing viral early genes E1A and E1B under TSTA (Ad-PSATSTAE1AE1B). When the two viruses are co-administered, we named the combination DTSTA for dual-TSTA system. LAPC-9 cells expressing Renilla luciferase were implanted subcutaneoulsy or in the peritoneum (i.p., as our local recurrence model) of scid/beige mice and tumor growth was monitored *in vivo* by bioluminescence. Intratumoral (i.t.) reporter activity was assessed after i.p. or i.t. injections of the viruses alone or in combination.

Results: In vitro, DTSTA infection of CWR-22Rv1 prostate cancer cells increased FL activity by 4.3-fold after 3 days when compared to Ad-PSATSTAfl alone. *In vivo,* i.t. injection of DTSTA in LAPC-9 tumors resulted in increased Ad-PSAPTSTAfl reporter activity by up to 25-fold (Fig. 1). Real-time PCR on tumor DNA confirmed viral genome replication in tumors infected with DTSTA. Finally, using an i.p. local recurrence after prostatectomy model, we show that DTSTAfl can detect and localize specifically prostate cancer cells.

Conclusion: We describe a new adenoviral based amplification system, named DTSTA, which can specifically detect prostate cancer cells by non-invasive imaging *in vivo*. If translated to the clinic, this nanotechnology could help treatment decision making when there is PSA recurrence after prostatectomy.

P5

Increased Cancer Cell Proliferation in Prostate Cancer Patients with High Levels of Serum Folate

Jeffrey J. Tomaszewski, *Jessica L. Cummings, Anil Parwani, Rajiv Dhir, Joel B. Mason, Joel B. Nelson, Dean J. Bacich, Denise S. O'Keefe*
University of Pittsburgh School of Medicine, Pittsburgh, PA, USA

Background: A recent clinical trial revealed that folic acid supplementation is associated with an increased incidence of prostate cancer. Given mandatory folic acid fortification of cereal grains in the United States, the potential link between prostate cancer and increased folic acid intake warrants further investigation

Objective: Determine the relationship between patient folate status and the proliferative capacity of Gleason 7 tumors in men with prostate cancer.

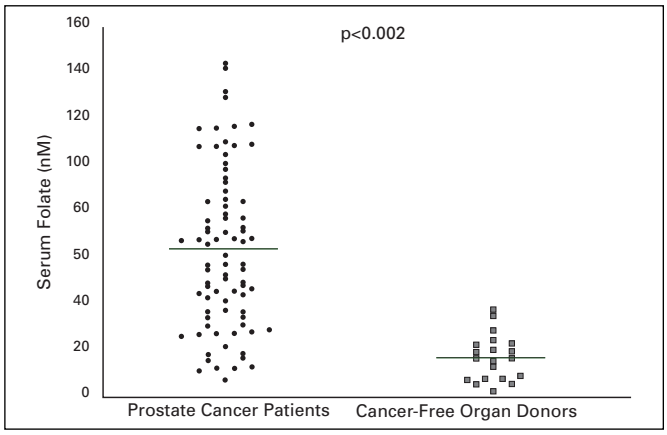

Fig. 1. P5. Fasting serum folate concentrations (nM) in patients with prostate cancer vs. cancer-free organ donors.

Methods: Serum and prostate samples from 86 patients undergoing surgery for prostate cancer and from 25 cancer-free organ donors were utilized to measure serum and/or prostate tissue folate concentrations, and assess Ki67 expression. Patients were assessed for genetic polymorphisms in methyltetrahydrofolate reductase and dihydrofolate reductase genes.

Results: Mean serum and tissue folate levels were significantly higher in men with prostate cancer compared to cancer-free organ donors ($p < 0.002$ and $p < 0.02$, respectively) (Fig. 1). Fasting serum folate levels were positively correlated with prostate cancer tissue folate content (n = 15; Spearman Correlation r = 0.577, $p < 0.03$). Fasting serum folate was significantly higher in users of folic acid supplements ($p < 0.05$). When divided into quartiles, there were no significant differences in serum folate levels between users and non-users of supplements. Among patients with Gleason 7 disease, the mean proliferation index was 6.17 ± 3.2% and 0.86 ± 0.92% in patients in the highest (117 ± 15nM) and lowest (18 ± 9nM) quintiles for serum folate, respectively ($p < 0.0001$) (Fig. 2).

Conclusions: This is the first report of a positive correlation between serum and prostate tumor folate. Increased cancer cell proliferation in men with higher serum folate concentrations is consistent with an increase in prostate cancer incidence observed with folate supplementation. Unexpectedly, more than 25% of our patients had serum folate levels greater than 6-fold adequate. Only half of these men reported supplement use, suggesting altered folate metabolism and/or consumption of folic acid from fortified foods.

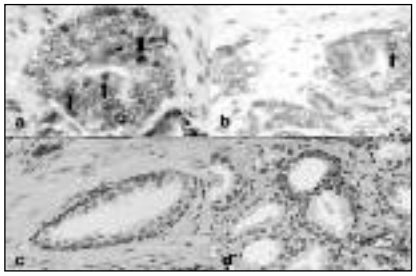

Fig. 2. P5. Representative light photomicrograph (63x) of Ki67 immunohistochemistry reveals significantly greater staining (arrows) in prostate cancer patients with high (a) vs. low (b) serum folate concentrations. Normal prostate glands from the same patients revealed no difference in Ki67 staining in patients with high (c) vs. low (d) serum folate concentrations.

P6

Nitric Oxide Signalling Mediates Hypoxic Upregulation of Macrophage Inhibitory Factor in Prostate Cancer

D. Robert Siemens
Queen's University, Kingston, ON, Canada

Background: Macrophage inhibitory factor (MIF) is an important chemokine influencing progression of prostate cancer. We have demonstrated that tumor hypoxia mediates many factors leading to a malignant phenotype in prostate cancer, including invasion, metastases and drug-resistance. Such hypoxia-induced phenotypes can be attenuated by manipulating nitric oxide (NO) signaling through classic, cGMP mediated pathways. The aim of this study was to determine the role of NO signalling in hypoxia-induced upregulation of MIF in prostate carcinoma cells.

Methods: MIF production by DU-145 prostate cancer cells (as well as the MDA breast cancer cell line) was determined by ELISA in different oxygen culture conditions (0.5-20% O_2). The role of NO signalling in hypoxia-mediated upregulation of MIF was determined by pharmacologic inhibitors and mimics of classic NO signalling with 10 nM GTN, 100 μM L-NMMA as well as non-hydrolysable analogue of cGMP, 8-bromo-cGMP (10 nM).

Results: These studies demonstrate that exposure of DU145 (as well as the MDA cell lines) to low oxygen tension for 24 hours consistently increased the secretion of MIF into the supernatant (1720 ± 245 ng/mL vs. 240 ± 46 ng/mL, $p < 0.05$). Incubation of the cell lines with the inhibitor of nitric oxide synthase L-NMMA in 20% oxygen resulted in a similar increase in MIF secretion (832 ± 66 ng/mL vs. 220 ± 33 ng/mL, $p < 0.029$). Restoring classical NO signalling in these cells with low concentrations of GTN or 8-bromo-cGMP was also able to significantly ($p < 0.05$) reverse the hypoxia-mediated increase in MIF.

Conclusions: These results contribute to our understanding of MIF regulation, an important chemokine linked to cancer progression in numerous cancer sites. It appears that decreased NO signalling, as a result of microenvironmental hypoxia, is at least partially responsible for increased MIF secretion by cancer cells. These results justify further *in vivo* investigations of the role of nitric oxide signalling and MIF action and may represent a novel target for pharmacologic therapy for prostate cancer.

P7

Reconstruction of a Human Vesical Equivalent Using Adipose-Derived Stem Cells

Alexandre Rousseau*, Jonathan Cloutier, Geneviève Bernard, Guillaume Marceau Fortier, Robert Gauvin, Sara Bouhout, Julie Fradette, Stéphane Bolduc*
LOEX, Centre de recherche FRSQ du CHA Universitaire de Québec, Université Laval, Québec, QC, Canada

Background: For several years, fibroblast cells have been primarily used for tissue engineering but adipose-derived stem/stromal cells (ASCs) show promising potential due to their facility to obtain, their capacity to differentiate and their ability to secrete mediators. Our group previously reported on the production of a bioengineered vesical equivalent using dermal fibroblasts without exogenous matrix. The aim of this study was therefore to evaluate the possibility of engineering an autologous vesical equivalent with human ASCs in order to validate if our model can benefit from the attributes of the ASCs.

Methods: ASCs were obtained from lipoaspirated adipose tissue and fibroblasts were extracted from a dermal biopsy. These human cells were cultured with serum and ascorbic acid to stimulate the formation of extracellular matrix and obtain cell sheets. Cells were cultured with constant media motion (GyrotwisterTM, Woodbridge, NJ) during three weeks and then three cell sheets of ASCs or fibroblasts were superimposed. After 4 days of maturation allowing cell sheet fusion, human urothelial cells were seeded on top of the construction and matured at the air/liquid interface. The vesical equivalents were characterized by histology, immunofluorescence as well as mechanical and suture resistance tests.

Results: Complete vesical equivalents were obtained with ASCs or fibroblasts. The histology clearly showed that cell sheets forming the ASC vesical equivalents featured a strong cohesion between cell sheets and were 1.8 fold thicker than the fibroblast vesical equivalents. Immunolabelings of the mature constructions showed the presence of cytokeratin 8\18, a differentiation marker for urothelial cell; and collagen 1 and 3, which are the major components of the extracellular matrix. The ASC vesical equivalents were easy to manipulate resistant enough to suture, therefore allowing the 3D reconstruction of a bladder shaped tissue engineered substitute.

Conclusions: Human vesical equivalents were successfully produced using either dermal fibroblasts or ASCs, without the use of exogenous scaffolding components. The ASC vesical equivalents could sustain suturing without tearing. Considering their accessibility, abundance and increased matrix production ACSs therefore represent a great cell source to further optimize our innovative model for vesical reconstruction.

P8

Stray Electrical Currents in Laparoscopic Instruments Used in DaVinci Robotic Surgery

Carlos E. Mendez Probst*,[1] George Vilos,[1] Paul Borg,[2] David Galloway,[2] Stephen E. Pautler[1]*
[1]Schulich School of Medicine and Dentistry, The University of Western Ontario, London, ON, Canada; [2]St Joseph's Health Care London, London, ON, Canada

Background: The use of the DaVinci robotic surgical system in laparoscopic procedures has gained wide acceptance and popularity across all surgical disciplines. This system however requires the utilization of monopolar electrosurgery and a finite reuse of electrosurgical instruments both of which provide opportunities for stray electrical currents from capacitive coupling and/or insulation failure. We report the prevalence and magnitude of such stray currents measured in DaVinci instruments that had reached the end of their duty cycle.

Methods: We tested 30 such instruments, 6 monopolar scissors, 1 Maryland bipolar forceps, 1 monopolar hook, 5 plasma kinetic dissecting forceps, 7 prograsp forceps, 10 large needle drivers using a Valleylab Force 2 ESU at pure coag and cut waveforms in open circuit at 4 different settings (open air) at 40 w, and sequentially gel coated instruments at 40 w, 80 w and maximum ESU output (coag 120 w, cut 300 w). The magnitude of stray currents was measured by an electrosurgical analyzer (454A Dynatec, Nevada). Visual inspection did not identify insulation defects in any of the instruments.

Results: At coag waveform in open air, 86% of instruments leaked a mean of 0.4 w (0-0.7 w). In the presence of gel coated instruments, stray currents were detected in all instruments with means and (range) of 4.2 w (1.5-7.7), 5 w (1.8-9.7), and 5 w (1.9-10.5) at 40 w, 80 w and 120 w, respectively. At cut waveform in open air, none of the instruments leaked current, while gel coated instruments leaked a mean of 2.7 w (0.6-4.3), 2.7 w (0.8-8.2) and 4 w (1.6-8.2) at 40 w, 80 w and 300 w, respectively. Compared by instrument group, the highest leakage was in PKDF (mean 4.1 w, one >8 w), followed by LND (3.3 w), PF (2.8 w), MBF (2.4 w), MCS (2.3 w), and MH (1.1 w).

Conclusions: At the end of their life cycle, all tested instruments showed energy leakage with one over 8 w, at >80 w of ESU power. Stray currents were higher during coag waveforms and the magnitude was not always proportionally related to ESU settings. Such stray currents may cause electrical burns to patients and/or operating room personnel.

P9

Vitamin D_3 Therapy Increases Cryoablation Efficacy: A Novel Strategy for the Treatment of Prostate Cancer

John M. Baust*,[1] Daniel Klossner,[2] Anthony Robilotto,[1] Robert Van Buskirk,[1] Andrew Gage,[1] Vladimir Mouraviev,[3] Thomas Polascik,[3] John G. Baust[2]*
[1]CPSI Biotech, Owego, NY, USA; [2]Binghamton University, Binghamton, NY, USA; [3]Duke University Medical Center, Durham, NC, USA

Introduction and Objective: Adjuvant therapies contribute to the successful treatment of cancer. Our previous reports have shown that combining cryoablation with cytotoxic agents enhances prostate cancer cell death. Vitamin D_3 (VD_3) is a natural steroidal hormone that has been

shown to exhibit cytotoxic properties preferentially inducing apoptosis in a variety of human cancer cells. Human prostate cancer cells are known to be resistant to many cytodestructive agents, including cryoablation and VD_3. Here, we evaluated the efficacy of VD_3 combined with cryoablation on androgen insensitive human prostate cancer (PC-3 and LNCaP-HP) cell death.
Methods: Freezing and VD_3 exposure to PC-3 and LNCaP-HP cells were performed using both 2D and 3D culture systems and efficacy was determined by cell viability assays. Resultant cell death and specific signaling components were determined using apoptotic inhibitors, fluorescence microscopy, protease activity assays and immunoblotting.
Results: Exposure of LNCaP-HP cells to freezing (-15°C) or VD_3 (50 uM) results in minimal cell death (15% and 10% respectively 3 days post treatment), while a complete loss of viability was observed with the combination. The synergistic effect was found to be due to a marked increase in apoptosis. Western blot analysis revealed a decrease in pro-caspase-9 and -3 between 6 and 18 hours post-exposure. Caspase activation assays confirmed the reduction in pro-caspase levels was a result of caspase activation. Protease inhibitors were incorporated into the combination protocol to determine the overall contribution of caspase activity in cell death. Inhibition of caspase-9 significantly blocked the combination induced cell death compared to cells that did not receive the inhibitor (55% vs. 21% viable, respectively). The addition of the caspase-8 inhibitor resulted in only minimal protection, indicating a specific mitochondrial-mediated event. Importantly, the combination was not effective when applied to normal prostate cells.
Conclusions: VD_3 sensitizes CaP cells to cryoablation. The significant increase in cell death was attributed to the activation of apoptosis, specifically through mitochondrial -mediated events. The results describe a novel therapeutic model for the treatment of prostate cancer and provide support for future *in vivo* studies.

P10

Rapid Induction of Apoptosis at Ultra Low Temperatures Enhances the Efficacy of Prostate Cancer Cryoablation

Anthony Robilotto,[1] *John M. Baust,[1] Robert VanBuskirk,[1] Andrew Gage,[1] John G. Baust[2]*
[1]CPSI Biotech, Owego, NY, USA; [2]Binghamton University, Binghamton, NY, USA

Introduction: Investigations into the molecular-based responses of prostate cancer following cold exposure have led to the discovery of delayed-onset, apoptotic cell death within the periphery of cryolesions. The apoptotic pathway typically attributed to this delayed death is the intrinsic/mitochondrial-mediated pathway characterized by a loss of mitochondrial potential, release of cytochrome c, and activation of caspase-9. Recent studies, however, have shown that at lower temperatures within the core of the cryogenic lesion (< -20°C) a rapid programmed cell death response occurs. Using an engineered, 3-dimensional prostate tumor model, we investigated these events to determine the signaling pathway(s) responsible for the cell death as a means of developing improved molecular based approaches for the cryoablation of prostate cancer.
Methods: Human prostate cancer cells (PC3) were cultured in the 3D matrices for 7 days prior to experimentation. The tumor models were then frozen to -30 or -15°C and analyzed at various times post-thaw using fluorescence microscopy, flow cytometry, and Western blots.
Results: Results demonstrated that the activation of apoptotic cell death occurred within 30 min of thawing at ultra low temperatures. At -30°C, ~25% of cells were apoptotic at 30 min and by 6 hr levels had dropped near those of controls. At elevated temperatures (-15°C), the activation and progression of apoptosis was considerably delayed, peaking at ~20% by 6 to 24 hr post-thaw. Additionally, it was determined that early onset apoptosis was regulated through a unique, caspase dependent process compared to that seen within the freeze margins. This induction was found to progress through a membrane mediated pathway associated with more severe thermal stressors as indicated by the activation of caspase-8 at low (-30°C) but not mild (-15°C) temperatures.
Conclusion: These data suggest that an apoptotic continuum exists throughout the cryolesion whereby the more severe the cryogenic stress, the faster programmed cell death is manifested. The identification of this rapid-onset apoptosis within the core of the ablative zone represents a novel finding in a region previously thought to be only necrotic. Ultimately, it is our aim to decipher the signaling pathways involved in triggering rapid-onset apoptosis such that these events can be manipulated to enhance cell death, thus improving the overall efficacy of cryosurgical procedures.

P11

The VHL Tumor Suppressor Promotes Renal Cancer Cell Apoptosis by Inhibiting Casein Kinase 2 Activity and Impairing NF-κB Signaling

Guan Wu, *Xiangrong He, Edward M. Messing*
University of Rochester, Rochester, NY, USA

Background: Renal cell carcinoma (RCC) responds notoriously poor to cytotoxic chemotherapy, indicating aberrant anti-apoptotic signal activation. Meanwhile, pVHL inactivation is implicated in most RCC cases, suggesting a potential link between pVHL and RCC apoptosis. In this report, we investigate abnormal anti-apoptotic behavior in pVHL-deficient RCC cells. Our objectives are to identify the molecular mechanism involved in RCC resistance to cytotoxicity-induced apoptotic signaling and to provide information that may lead to better RCC treatment design.
Methods: HEK293, Hela, and RCC cell lines, including 786-O, RCC4, cell lines derived from these two cell lines were used in our experiments. The GST pull-down and co-IP assays were conducted to confirm protein interactions. Western blotting was performed for evaluating protein expression/activation. Kinase activity was measured by in vitro kinase assay. NF-κB activation was dedected by EMSA and luciferase reporter gene assay. RNAi techniques were applied for transient knockdown of specific protein expressions and for the construction of RNAi stable RCC cell lines. Apoptosis was assessed via FACS or fluorescence microscope.
Results: In this study, we found that pVHL inhibits NF-κB activity by interacting with casein kinase 2α (CK2α), an I B-independent pathway. The CK2α protein level was not regulated by pVHL or hypoxia. Upon TNFα treatment, pVHL-deficient RCC cells exhibit much stronger NF-κB activation and dramatically elevated resistance to apoptosis. pVHL-deficient RCC cells also showed increased NF-κB p65 serine529 phosphorylation and enhanced association between p65 and CBP/p300. Knockdown of CK2α in pVHL-deficient RCC cells inhibited p65 ser529 phosphorylation and abnormal NF-κB activation and blunted NF-κB downstream anti-apoptotic gene expressions, which lead to restored sensitivity to TNFα-induced apoptosis. Moreover, a chemical inhibitor of CK2, 5,6-dichlororibifuranosylbenzimidazole (DRB) also showed robust inhibition of abnormal NF-κB activation in pVHL-deficient RCC cells.
Conclusions: Our findings suggest that pVHL regulate NF-κB anti-apoptotic pathway by suppressing CK2 kinase activity and p65 serine529 phosphorylation - a process that culminates in decreased p65/p300/CBP interaction and enhanced RCC apoptosis. This represents a novel mechanism of how pVHL inactivation reduces RCC cells susceptibility to cytotoxicity-induced apoptosis by promoting CK2 and NF-κB activations.

P12

The Effect of Dietary Folate on Prostate Carcinogenesis in an *in vivo* Model of Tumorigenesis

Jeffrey J. Tomaszewski, *Jessica L. Cummings, Anil Parwani, Dean J. Bacich, Denise S. O'Keefe*
University of Pittsburgh School of Medicine, Pittsburgh, PA, USA

Introduction: Recent studies demonstrate that folic acid supplementation is associated with an increased incidence of prostate cancer. We previously reported a positive correlation between serum and prostate tumor folate, and increased cancer cell proliferation in men with higher serum folate concentrations.
Objective: To determine the effect of dietary folate manipulation on prostate carcinogenesis and progression in an *in vivo* model of tumorigenesis.

Table 1. P12.

	Epithelium (dietary folate intake mg/kg)	Normal	Hyperplasia	PIN	Small atypical foci with features of adenocarcinoma
8 weeks	Normal (0)	2/8 (25%)	5/8 (63%)	1/8 (13%)	0/8 (0%)
	Tumor (0)	1/6 (17%)	0/6 (0%)	3/6 (50%)	2/6 (33%)
	Normal (2)	2/6 (33%)	3/6 (50%)	1/6 (17%)	0/6 (0%)
	Tumor (2)	0/4 (0%)	0/4 (0%)	2/4 (50%)	2/4 (50%)
	Normal (20)	0/7 (0%)	4/7 (57%)	3/7 (43%)	0/7 (0%)
	Tumor (20)	0/11 (0%)	0/11 (0%)	8/11 (73%)	3/11 (23%)
16 weeks	Normal (0)	1/12 (8%)	10/12 (84%)	1/12 (8%)	0/12 (0%)
	Tumor (0)	2/16 (13%)	3/16 (19%)	2/16 (13%)	9/16 (55%)
	Normal (2)	2/12 (17%)	6/12 (50%)	3/12 (25%)	1/12 (8%)
	Tumor (2)	0/8 (0%)	1/8 (12%)	5/8 (63%)	2/8 (25%)
	Normal (20)	2/7 (29%)	4/7 (57%)	0/7 (0%)	1/7 (14%)
	Tumor (20)	0/7 (0%)	0/7 (0%)	6/7 (86%)	1/7 (14%)
24 weeks	Normal (0)	0	0	0	0
	Tumor (0)	1/4 (25%)	0/4 (0%)	1/4 (25%)	2/4 (50%)
	Normal (2)	2/4 (50%)	1/4 (25%)	0/4 (0%)	1/4 (25%)
	Tumor (2)	0/6 (0%)	0/6 (0%)	4/6 (67%)	2/6 (33%)
	Normal (20)	0/8 (0%)	5/8 (63%)	3/8 (37%)	0
	Tumor (20)	0	0	0	0

PIN = prostatic intraepithelial neoplasia.

Methods: Utilizing the subrenal prostatic recapitulation model for tissue recombination, rat urogenital mesenchyme (rUGM) was microdissected from rat embryos and combined with 10-20 mg slivers of prostate tumor or normal prostate tissue from patients with prostate cancer. Tissue recombinants were grafted beneath the renal capsule of male SCID mice. Mice were treated hormonally at the time of grafting with testosterone propionate and 17β-estradiol. Mice were randomly assigned to receive amino-acid defined diets which were folate-deficient (0 mg/kg), folate-sufficient (2 mg/kg), or excessively folate-fortified (20 mg/kg). Tissue recombinants were serially grafted and harvested after 8, 16, and 24 weeks under the renal capsule. Histological and morphological features were assessed based upon 20 fields per recombinant, with the worst histological phenotype assigned to that recombinant. Immunohistochemical analysis to detect basal cells (p63), proliferation (Ki67), DNA methylation (5-methylcytosine), and tumor aggressiveness (EZH2) was performed.
Results: Recombinants from normal and cancerous prostate tissue formed normal, hyperplastic, focal PIN like glandular structures, and adenocarcinoma. The incidence of normal glands, hyperplasia, PIN, and adenocarcinoma in human prostate cancer tissue recombinants was 6.5%, 6.5%, 50% and 37%, respectively; incidence in normal prostate tissue recombinants was 17%, 62.5%, 18.7%, and 4.7% (Table 1). Among normal prostate tissue recombinants, excess dietary folate intake increased the incidence of PIN and adenocarcinoma when compared to recombinants grown in mice receiving a folate deficient diet (31.3% vs. 7%, respectively; $p < 0.05$). An increased incidence of PIN and adenocarcinoma was also observed among prostate cancer recombinants in mice with adequate or excess dietary folate intake when compared to folate deficient mice (97.6% vs. 75.3%, respectively; $p < 0.05$).
Conclusions: Adequate to excess levels of dietary folate promote prostate carcinogenesis compared to folate deficiency in an in vivo human prostate tissue recombinant model of tumorigenesis.

P13

Nox4 is Required for Nuclear Translocation of HIF-2α in Renal Cancer Cells

Guimin Chang, *Li Chen, Jodi K. Maranchie*
University of Pittsburgh Medical Center, Pittsburgh, PA, USA

Background: Renal cell carcinoma (RCC) causes nearly 12,000 deaths each year in America. Nox4 belongs to the NADPH oxidase family that generates reactive oxygen species (ROS). The kidney is the site of greatest abundance of the Nox4. We previously showed that Nox4 is critical to activation of HIF-2α and necessary to support the tumor phenotype of RCC cells. However, the mechanism of Nox4 induction of HIF-2α is unknown. Inactive HIF-2α is located in the cytoplasm and activation requires translocation to the nucleus where it dimerizes with ARNT and binds DNA. To determine if Nox4 is required for nuclear translocation, we localized exogenous HIF-2α by immunofluorescence in RCC cells in the presence or absence of Nox4. We further mutated key HIF-2α hydroxylation sites to measure their impact on translocation.
Methods: 786-0 human kidney cancer cells with stable expression of Nox4 shRNA (KD) or a non-targeting shRNA (NS) were transiently transfected with pSNAP- HIF-2α to express wild type HIF-2α tagged at the N-terminus with SNAP. Cells were cultured 48 hr under 21% or 1% oxygen conditions and then fixed and bound to an anti-SNAP primary antibody. Nuclei were counterstained with DAPI. pSNAP- HIF-2α-PA was cloned by site directed mutagenesis of Pro531 to Ala, and pSNAP-HIF-2α-NA, was derived by mutation of Asp851 to Ala.
Results: 786-0 NS cells showed moderate nuclear HIF-2α localization at 21% O_2 with a shift to 100% nuclear expression under hypoxia. With Nox4 silencing, the 786-0 KD cells demonstrated only cytoplasmic localization regardless of oxygen conditions, suggesting that Nox4 is critical to HIF-2α nuclear translocation in normoxia or hypoxia. HIF-2α-PA mutation did not alter the localization pattern at 21% or 1% O_2. HIF-2α-NA mutants, however, demonstrated cytoplasmic localization under all conditions. HIF-2α staining intensity was significantly lower in KD than NS. Addition of the proteasome inhibitor, MG132 (0.1 M) increased staining intensity to levels seen in 786-0 NS.

Conclusions: We show for the first time that Nox4 expression is required for HIF-2α nuclear translocation in RCC cells under both hypoxic and non-hypoxic conditions. Asp851 appears to be required for Nox4-mediated translocation. We speculate that Nox4-derived ROS may inhibit FIH, the enzyme responsible for Asp851 hydroxylation, thereby triggering this "hypoxic switch" in the absence of hypoxia. Furthermore, stabilization of HIF-2α by proteasome inhibitors suggests that Nox4 protects HIF-2α from proteasomal degradation via a pVHL-independent pathway. Ongoing investigations aim to further elucidate these pathways.
Funding: ACS RSG-09-023-01-CNE

P14

Temporal RF-Ultrasound Augmentation of Prostate (TRAP): Enhancing Prostate Cancer Detection Utilizing Temporal Ultrasound Radio Frequency Signals

***D. Robert Siemens**, Purang Abolmaesumi, Parvin Mousavi, Mehdi Moradi, Eric Sauerbrei, Sandy Boag*
Queen's University, Kingston, ON, Canada

Background: Ultrasound echo signals are affected by the geometrical deregulation of cellular architecture in neoplastic tissue and can be exploited to differentiate normal from various grades of cancerous tissue, information that is not visible in post-processed B-scan ultrasound images. We have proposed to apply an innovative approach to process raw transrectal ultrasound (TRUS) radio-frequency (RF) signals for the early detection of prostate cancer.
Methods: *Ex vivo* experiments have involved evaluation of a time series, through fractal and frequency analyses, of raw temporal RF ultrasound signals to differentiate tissue types in 35 human prostates obtained after radical prostatectomy. Previously described ultrasound texture features for tissue typing were included in these studies for comparison. Detailed whole mount sectioning of the prostate specimens were regarded as the gold standard and compared to probability maps created by analysis of the temporal RF signals.
Results: Comparing the generated probability maps of prostates scanned ex vivo to the detailed pathology reports have demonstrated sensitivity and specificity values of 90% and 85% respectively, in characterizing cancerous tissue. The area under receiver operating characteristic curve for the subset of RF time series evaluation was 0.87, which increased to 0.95 when combined with other ultrasound texture features. Validation utilizing leave one patient out resulted in an area under the curve of 0.82.
Conclusions: These results suggest that the temporal ultrasound echo signals can be employed to differentiate different tissues in the prostate and subsequently improve cancer detection. Furthermore, we propose to train classifiers in order to visualize this information as color-coded probability maps on real-time US images and have initiated an in vivo study for men undergoing TRUS guided biopsy.

P15

Urinary MicroRNA As An Accurate Urinary Diagnostic Marker For Urothelial Cancer

***D. Robert Siemens**, Jaime Snowden, Jason Izard, Sandy Boag, Harriet Feilotter*
Queen's University, Kingston, ON, Canada

Background: MicroRNAs (miRNAs) are a class of small RNAs that are important regulatory molecules, involved in several cell processes such as developmental timing, stem cell division, and apoptosis. Dysregulated miRNAs have been identified in several human malignancies, including bladder cancer tissue samples, and may confer a "tumor signature" that can be exploited for diagnostic purposes. We report on a prospective pilot study investigating the diagnostic capability of miRNAs in the urine of patients with urothelial cancer.
Methods: Voided urine samples were collected from 8 patients with urothelial carcinoma just prior to bladder tumor resection as well as 5 age-matched healthy control patients. Pathology demonstrated both low grade and high-grade cancer. Total RNA was isolated and quantitative reverse transcriptase-polymerase chain reaction was performed on the RNA extracts using primers for 4 miRNAs shown previously to be dysregulated in solid urothelial carcinomas with RNU6B as the endogenous control. Standard urine cytology was performed on all samples in a blinded fashion.
Results: Two miRNAs were found to be significantly dysregulated in the urine from cancer patients with miR-A showing an average 10.42-fold decrease ($p < 0.05$) and miR-B showing an average 2.70-fold increase ($p > 0.05$) in the cancer samples compared to the normal controls. Using these 2 miRNAs, a decision-tree prediction model was generated yielding a specificity of 100% and a sensitivity of 87.5%. The sensitivity and specificity of the cytology on the same urine samples was 50% and 80% respectively.
Discussion: MiRNA expression levels are altered in bladder cancer and may have diagnostic and prognostic value. This preliminary study of candidate urinary miRNA in patients with both low grade and high-grade urothelial cancer demonstrated a significantly improved diagnostic accuracy over cytology. These results provide rationale for further studies on discovery and validation of candidate miRNAs in voided urine and may potentially lead to the development of a non-invasive and sensitive test for bladder cancer diagnosis and prognosis.

P16

Development of a Realtime Intraoperative Electrical Impedance Tomography Sensor for Cavernous Nerve Mapping for Radical Prostatectomy

Henry H. Tran
University of British Columbia, New Westminster, BC, Canada

Introduction and Objective: Radical prostatectomy is a proven efficacious treatment locally confined prostate cancer, however rates of post operative impotency continue to range between 10-30% in contemporary series. Thus, in addition to satisfactory cancer control, accurate localization of the cavernous nerves and the contributing plexus during resection is exceedingly important during radical prostatectomy. We have developed a realtime, intraoperative tissue impedance sensor for nerve localization based on electrical impedance tomography (EIT) technology, which will serve to reduce post prostatectomy impotence
Methods: The prototype constructed consists of a probe with a needle array to interface with the tissue, and a signal generator and analysis system. The device cycles through each set of electrodes on the probe, and injects current while simultaneously computing the voltage change. Reconstruction algorithms determine nerve location based on tissue impedance properties. The system was functionally validated in an in vitro model system and following further refinement, rat sciatic nerve identification. For each trial, the probe was placed on the tissue and the device sequentially injected 5mA sinusoidal current across each of its electrodes with the resulting voltages recorded.
Results: Each trial demonstrated the ability of the device to detect changes in impedance of different tissues. Electrodes closest to the wire in the in vitro model had the smallest voltage change, corresponding to a lower impedance value. V=0.135V for the electrodes near the wire, compared to V=0.256V for other electrodes. Localization of rat sciatic nerve was also successful demonstrating V=0.294V for the electrodes near the nerve, compared to V=0.467V for the remaining electrodes.
Conclusions: We have developed a realtime intraoperative tissue sensor prototype based on electrical impedance tomography which has demonstrated early proof of principle success in in vitro and small animal models of mixed tissue determination and nerve localization. With further refinements in both probe array fabrication and miniaturization as well as digital signal processing we believe this device may deliver significant benefit to procedures such as radical prostatectomy where nerve structures may be visually indeterminant but critical for preservation of function.

P17

Mapping the Cytokine Profile of Interstitial Cystitis in Human Bladder and Urine Specimens: A Pilot Study

Anthony T. Corcoran,[1] *Vikas Tyagi,*[1] *Masa Kita,*[1] *Pradeep Tyagi,*[2] *Wendy W. Leng,*[1] *Naoki Yoshimura*[1]

[1]University of Pittsburgh Medical Center, Pittsburgh, PA, USA, [2]William Beaumont Hospital, Royal Oak, MI, USA

Introduction: Evidence suggests that increases in cytokine activity may be involved in the pathogenesis of painful bladder syndrome/interstitial cystitis (PBS/IC). However, data on cytokine activity in human PBS/IC patients are lacking. This pilot study investigated the cytokine profile in human bladder tissue and urine of PBS/IC patients.

Methods: Ten PBS/IC patients (ICS definition) were enrolled in this pilot study. Human bladder (cold cup biopsy) and urine specimens were collected intraoperatively before hydrodistention (HD) under general anesthesia. Follow-up urine was also collected post-HD (mean 27 days). Specimens were compared to a control group of banked human bladder tissue and urine specimens (n = 10) from non-PBS/IC patients. A comparison of 22 cytokines was performed using multiplex analysis with a multiple antigen bead assay (Luminex 100 IS). Statistical analysis was performed using two-tailed t-tests ($p \leq 0.5$).

Results: Compared to control bladder tissue specimens; IL-16, IL-18, CTACK, ICAM-1, MCP-3, SCGFb, TRAIL and VCAM1 were significantly elevated in PBS/IC bladder tissue. When comparing the cytokine profile of control and pre-HD PBS/IC urine specimens, no significant differences were noted. However, when comparing pre-HD and post-HD urine specimens within the PBS/IC patients; MCP-3 and TRAIL were noted to be significantly decreased after hydrodistension. Standardized measures of clinical symptoms (pain, urgency and frequency (PUF) overall score [mean 25.8 ± 5.5 vs. 20.3 ± 7, $p = 0.04$] and PUF symptom score [mean 18.2 ± 3.2 vs. 12.2 ± 5.9; $p = 0.009$]) showed improvement in the pre- and post-HD comparison.

Conclusions: These results indicate that several cytokines are significantly elevated in PBS/IC bladder tissue. Of these cytokines, MCP-3 and TRAIL appear to significantly decrease in urine specimens in association with clinical improvement (as measured by PBS/IC symptom scores) after HD treatment in PBS/IC patients and may candidates for biomarkers. Further larger-scale studies are needed to map the cytokine profile in PBS/IC.